Flexible Fast-Convolution Processing for Cellular Radio Evolution

Juha Yli-Kaakinen, Toni Levanen, Arto Palin, Markku Renfors, *Life Fellow, IEEE*, and Mikko Valkama, *Fellow, IEEE*

***Abstract*— Orthogonal frequency-division multiplexing (OFDM) has been selected as a baseline waveform for long-term evolution (LTE) and fifth-generation new radio (5G NR). Fast-convolution (FC)-based frequency-domain signal processing has been recently considered as an effective tool for transmitter and receiver side subband filtering of OFDM-based waveforms. However, for the original continuous FC-based model, the filtering can, in general, be configured in time-direction only with the granularity of half subframe, corresponding to 7, 14, or 28 symbols with 15 kHz, 30 kHz, or 60 kHz subcarrier spacing, respectively. In this paper, we present a symbol-synchronous FC-processing scheme flexibly allowing filter re-configuration with the time resolution equal to one OFDM symbol while supporting tight carrier-wise filtering for 5G NR in mixed-numerology scenarios with adjustable subcarrier spacings, center frequencies, and subband bandwidths, as well as providing co-existence with LTE. Proposed approach segments each stream of time-domain OFDM symbols into overlapping processing blocks of fixed size. Symbol synchronous processing is achieved by dynamically adjusting the overlap between the processing blocks while aligning the payload part of the processing blocks with the boundaries of the OFDM symbols. The proposed scheme is demonstrated to support the envisioned use cases of 5G NR and provide a flexible starting point for sixth generation (6G) development.**

***Index Terms*— Filtered-OFDM, multicarrier, waveforms, fast-convolution, physical layer, 5G, 5G New Radio, 5G NR, guard-band IoT, LTE-NR coexistence, 6G.**

I. Introduction

ORTHOGONAL frequency-division multiplexing (OFDM) is utilized in long-term evolution (LTE) and fifth-generation new radio (5G NR) due to its high flexibility and efficiency in allocating spectral resources to different users, simple and robust way of channel equalization, as well as simplicity of combining multiantenna schemes with the core physical-layer processing [1]. The poor spectral localization of the OFDM, however, calls for enhancements such as time-domain windowing or filtering to improve the localization of the waveform by effectively suppressing the unwanted emissions. This is important especially in challenging new spectrum use scenarios like asynchronous multiple access, as well as in mixed-numerology cases aiming to use adjustable symbol and cyclic prefix (CP) lengths, subcarrier spacings (SCSs), and frame structures depending on the service requirements [2], [3], [4], [5], [6].

In general, the objective of the windowing or filtering is to improve the spectral utilization of the channel by improving the localization of the waveform in frequency direction, that is, maximizing the transmission bandwidth for a given channel bandwidth. Time-domain filtering-based approaches can be utilized for considerably reducing the spectral leakage of the OFDM waveforms. However, long filters, typically of the order of half the symbol duration, are needed [5]. This makes the dynamic re-configuration, e.g., changing the filter bandwidth, practically impossible due to the long filter transients. In addition, the latency introduced by long filters, require long turn-around times in time-division duplex (TDD) scenarios. The complexity of the time-domain convolution becomes also the bottleneck as no effective structures exist for non-uniform filter banks required for supporting arbitrary transmission bandwidths and center frequencies. On the other hand, time-domain windowing, in general, has very low complexity but its performance is quite limited, especially for high subcarrier spacings with relatively short CP durations.

Fast-convolution (FC)-based filtering has been recently proposed as an efficient tool for spectrum control of singe-carrier and multi-carrier waveforms [7], [8], [9], [10], [11], [12], [13], [14], [15], [16], [17], [18]. FC-based filter-bank solutions have superior flexibility when compared with the conventional time-domain polyphase-type filter banks [19]. FC processing approximates a linear (aperiodic) convolution through effective fast Fourier transform (FFT)-based circular convolutions using partly overlapping processing blocks (so-called FC blocks). With FC processing, it is very straightforward to adjust individually the bandwidths and center frequencies of the subbands with possibly different numerologies [12], even at the symbol level.

In the original *continuous* FC-based filtered-OFDM processing model derived in [10] and [12], continuous stream of CP-OFDM symbols are divided into overlapping

Manuscript received 1 January 2022; revised 3 June 2022 and 5 August 2022; accepted 4 September 2022. Date of publication 15 September 2022; date of current version 18 November 2022. This work was supported in part by the Business Finland (formerly known as the Finnish Funding Agency for Innovation, Tekes) and Nokia Bell Labs through the Projects 5G-VIIMA and 5G-FORCE; in part by Nokia Networks; and in part by the Academy of Finland under Project #284694, Project #284724, Project #319994, and Project #338224. The associate editor coordinating the review of this article and approving it for publication was B. Shim. *(Corresponding author: Juha Yli-Kaakinen.)*

Juha Yli-Kaakinen and Toni Levanen are with Nokia Networks, FI-33100 Tampere, Finland (e-mail: juha.yli-kaakinen@nokia.com; toni.a.levanen@nokia.com).

Arto Palin is with Microsoft, FI-33100 Tampere, Finland (e-mail: arto.palin@gmail.com).

Markku Renfors and Mikko Valkama are with the Department of Electrical Engineering, Tampere University, FI-33101 Tampere, Finland (e-mail: markku.renfors@tuni.fi; mikko.valkama@tuni.fi).

Color versions of one or more figures in this article are available at https://doi.org/10.1109/TCOMM.2022.3206889.

Digital Object Identifier 10.1109/TCOMM.2022.3206889

FC-processing blocks of the same size and the overlap between FC blocks is fixed (typically 50%). Since the CP length in 5G NR is non-zero and both the OFDM symbol length and the FC-processing block size typically take power-of-two values, the FC blocks are not time synchronized to CP-OFDM symbols. The drawback of this approach is that, when the filter configuration changes, e.g., when the bandwidth or center frequency of the subband (or bandwidth part (BWP) in the 5G-NR terminology) is modified, then this change typically occurs within a FC-processing block, which degrades the filtering performance during this block.

In *discontinuous symbol-synchronized* FC processing as detailed in [13] and [16], each symbol is divided into fixed number of processing blocks (e.g. two). These FC-processing blocks are then filtered using FC-based circular convolutions and the filtered FC-processing blocks are concatenated by using overlap-and-add (OLA) processing to form a stream of filtered CP-OFDM symbols. In this case, the change in filtering configuration does not induce any additional intrinsic interference, since the OFDM symbol boundaries are also boundaries of the payload part of the FC blocks. However, for this approach, the FC processing blocks are aligned only with one numerology at a time, which induces problems in supporting mixed numerology. Also, the needed OLA scheme may introduce additional constrains in ultra-reliable low-latency communications (URLLC) due to the overlapping needed at the output side.

In *continuous symbol-synchronized* processing model proposed in this article, the continuous stream of symbols is divided into overlapping blocks such that the overlap and the block locations are dynamically adjusted based on the CP lengths, thus guaranteeing the synchronous processing of all CP-OFDM symbols for all numerologies with normal CP. Therefore, the proposed approach avoids the drawbacks of the original continuous and discontinuous symbol-synchronized FC-based filtered-OFDM models. The only drawback is that the smallest possible forward transform size is somewhat higher when compared to earlier approaches.

The main contributions of this paper can be summarized as follows:

- Symbol-synchronized processing is proposed, where the processing blocks are aligned with OFDM symbols of all different subcarrier spacings in mixed-numerology implementation of 5G NR physical layer. The processing blocks are also aligned between LTE and all numerologies of 5G NR, allowing smooth carrier combining processing in multi radio access technology (RAT) or multi-radio transmitter (TX) and corresponding carrier separating receiver (RX) processing.
- The proposed processing is shown to support dynamic changes in filter parameterization with the time resolution equal to the the duration of the shortest symbol in 5G NR numerology, thus allowing the most flexible allocation of resources in time and frequency directions.
- FC-processing models are developed for both overlap-and-save (OLS) and OLA (and even mix of these), providing an additional degree of flexibility for implementations.
- The proposed frequency-domain (FD) processing is shown to provide wide-band subband-wise (fractional) delay adjustments, e.g., to compensate the delays in other parts of the processing chain.

The presented solution supports all different use cases envisioned for the flexible BWP-based 5G-NR radio interface, allowing filter re-configuration with time resolution equal to one OFDM symbol, while maintaining high quality separation of different frequency blocks. Existing reference methods in [13], [16], and [12] and time-domain filtering-based methods in general do not allow the same flexibility in allocating the resources in time- and frequency directions. The solutions presented here are especially important for below-7 GHz communications due to scarce spectral resources, but there is no limitation in applying the solutions also for higher carrier frequencies if seen useful. One concrete example is the frequency range of 7–20 GHz that is likely to be deployed in future 6G networks.

The remainder of this paper is organized as follows. Section II shortly reviews the 5G NR numerology and relevant terminology for reference. Then, the proposed continuous symbol-synchronized FC-based filtered-OFDM processing models for TX and RX are described in Section III. Section IV introduces the key metrics and requirements used for evaluating the performance of the TX processing. In Section V, the performance of the proposed processing is demonstrated in various mixed-numerology scenarios. Finally, the conclusions are drawn in Section VI.

Notation and Terminology

In the following, boldface upper and lower-case letters denote matrices and column vectors, respectively. $\mathbf{0}_{q\times p}$ and $\mathbf{1}_{q\times p}$ are the $q \times p$ matrices of all zeros and all ones, respectively. $\mathbf{I}_q$ and $\mathbf{J}_q$ are the identity and reverse identity matrices of size q. The entry on the ith row and jth column of a $q\times p$ matrix $\mathbf{A}$ is denoted by $[\mathbf{A}]_{i,j}$ for $i \in \{0,1,\ldots,q-1\}$ and $j \in \{0,1,\ldots,p-1\}$ and $[\mathbf{A}]_j$ denotes the jth column of $\mathbf{A}$. For vectors, $[\mathbf{a}]_j$ denotes the jth element of $\mathbf{a}$. The column vector formed by stacking vertically the columns of $\mathbf{A}$ is $\mathbf{a} = \mathrm{vec}(\mathbf{A})$. Furthermore, $\mathrm{diag}(\mathbf{a})$ denotes a diagonal matrix with the elements of $\mathbf{a}$ along the main diagonal. The transpose of matrix $\mathbf{A}$ or vector $\mathbf{a}$ is denoted by $\mathbf{A}^{\mathsf{T}}$ and $\mathbf{a}^{\mathsf{T}}$, respectively, while the corresponding conjugate transposes are denoted by $\mathbf{A}^{\mathsf{H}}$ and $\mathbf{a}^{\mathsf{H}}$, respectively. The Euclidean norm is denoted by $\|\cdot\|$ and $|\cdot|$ is the absolute value for scalars and cardinality for sets. Element-wise (Hadamard) product is denoted by $\odot$.

II. 5G New Radio Scalable Numerology and Frame Structure

This section summarizes the 5G-NR numerology and frame structure in order to illustrate the needed flexibility in time and frequency directions required by the filtering solutions to support most challenging use cases.

CP-OFDM has been selected as the baseline waveform for 5G NR at below 52.6 GHz frequency bands, while

TABLE I
5G-NR MIXED NUMEROLOGY IN FREQUENCY RANGE 1 (FR1)

Subcarrier spacing, $f_{\mathrm{SCS},m,n}$	15 kHz	30 kHz	60 kHz	$2^{\mu}\times 15$ kHz
OFDM symbol duration, $T_{\mathrm{OFDM},m,n}$	66.7 µs	33.3 µs	16.7 µs	$2^{-\mu}\times 66.6$ µs
Cyclic prefix duration, $T_{\mathrm{CP},m,n}$	4.69 µs	2.34 µs	1.17 µs	$2^{-\mu}\times 4.69$ µs
Number of OFDM symbols per slot, $N^{\mathrm{symb}}_{\mathrm{slot}}$	14	14	14 or 12	14 or 12
Number of slots per subframe, $N^{\mathrm{slot}}_{\mathrm{subframe}}$	1	2	4	2^{μ}
Slot duration, T_{slot}	1 ms	0.5 ms	0.25 ms	$2^{-\mu}\times 1$ ms

DFT-spread-OFDM (DFT-s-OFDM) (also known as single-carrier frequency-division multiple access (SC-FDMA)) can also be used for uplink (UL) in coverage-limited scenarios. 5G NR provides scalable numerology and frame structure in order to support diverse services, deployment scenarios, and user requirements operating from bands below 1 GHz to bands above 30 GHz known as millimeter-wave (mmWave). This numerology supports multiple SCSs in order to reduce latency and to provide increased robustness to phase noise and Doppler, especially at higher carrier frequencies. In addition, by increasing the SCS, the maximum channel bandwidth supported for a given OFDM transform size can be increased. On the other hand, smaller SCSs have the benefit of providing longer CP durations in time and, consequently, better tolerance to delay spread with reasonable overhead [1]. These smaller SCSs also allow transmitters to increase the power spectral density of the transmitted signal, which can be used for extending 5G-NR coverage.

5G NR supports subcarrier spacings (SCSs) of $2^{\mu}\times 15$ kHz where $\mu = 0, 1, \ldots, 4$ while only 15 kHz is supported by LTE. Similar to LTE technology, a radio frame of 10 ms is divided into 10 subframes, each having 1 ms duration while each subframe has 2^{μ} slots. Each slot consists of either 14 or 12 OFDM symbols for the normal CP or extended CP, respectively [1], [20]. The slot duration varies based on the SCS as $T_{\mathrm{slot}} = 2^{-\mu}\times 1$ ms. The numerology for 15 kHz, 30 kHz, and 60 kHz SCS is summarized in Table I. Fig. 1 exemplifies the time alignment of different numerologies within a half subframe. In general, 5G NR does not specify the minimum number of consecutive symbols of certain SCS and, therefore, in extreme time-multiplexing cases, it is possible that the SCS changes even at the symbol level as illustrated in Fig. 1(d).

5G NR supports also non-slot based scheduling (so-called mini slots), where the transmission length can be configured between 1 and 13 symbols [21, Sec. 8.1]. This mini-slot concept is especially essential for URLLC and for dynamic time-domain multiplexing. Such transmissions can pre-empt the ongoing slot-based transmission and, therefore, also the time-domain flexibility of the filtering solutions becomes crucial in the 5G-NR context.

5G NR allows the use of a mixed numerology, i.e., using different SCSs in different subbands (or BWPs) within a single channel. However, the use of different SCSs within an OFDM multiplex harms the orthogonality of subcarriers, introducing inter-numerology interference (INI). To cope with INI in mixed-numerology scenarios with basic CP-OFDM waveform, relatively wide guard bands (GBs) should be applied between adjacent BWPs, which would reduce the spectral efficiency. Alternatively, the third generation partnership project (3GPP) allows to use spectrum enhancement techniques for CP-OFDM, but this should be done in a transparent way and without performance loss with respect to plain CP-OFDM. The transparency means that a TX or a RX does not need to know whether spectrum enhancement is used at the other end. The spectrum enhancement techniques should also be compatible with each other, allowing different techniques to be used in the TX and RX. Transparent enhanced CP-OFDM techniques have been considered in [22], [23], and [24].

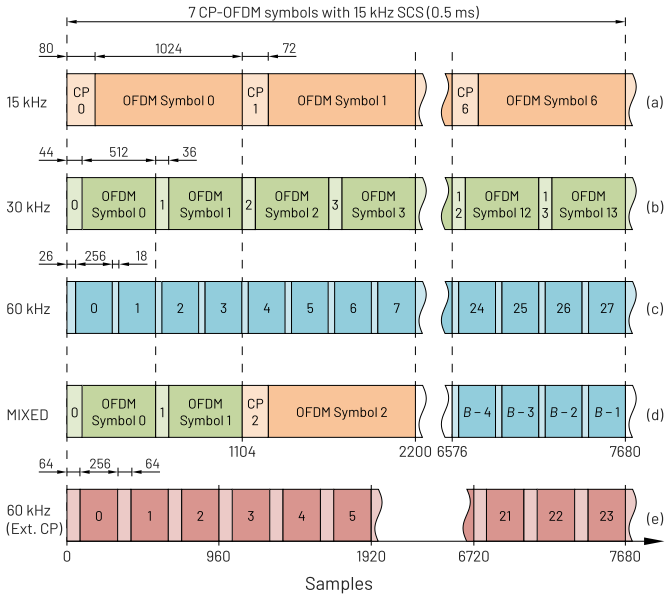

Fig. 1. Illustration of multiple numerologies in 10 MHz channel and their synchronization within the half subframe (0.5 ms). (a)–(c) 15 kHz, 30 kHz, and 60 kHz SCS with normal CP, respectively. (d) Time-multiplexed mixed numerology case. (e) 60 kHz SCS with extended CP.

TABLE II
NOMINAL CHANNEL BANDWIDTHS ($f_{\mathrm{Ch,BW}}$) FOR 5G-NR FREQUENCY RANGE 1 (FR1) AND CORRESPONDING SAMPLE RATES (f_{s})

$f_{\mathrm{Ch,BW}}$ [MHz]	5.00	10.00	15.00	20.00	25.00	30.00	40.00
f_{s} [Msps]	7.68	15.36	23.04	30.72	30.72	46.08	61.44
$f_{\mathrm{Ch,BW}}$ [MHz]	50.00	60.00	70.00	80.00	90.00	100.00	
f_{s} [Msps]	61.44	92.16	92.16	122.88	122.88	122.88	

Let f_{s} be the OFDM waveform sample rate as tabulated in Table II for 5G-NR channel bandwidths

TABLE III

NOTATIONS USED FOR DENOTING THE NUMEROLOGY. SUBSCRIPT m DENOTES THE SUBBAND INDEX AND n DENOTES THE OFDM-SYMBOL INDEX

Notation	Dim.	Description
f_{s}	$\mathbb{R}$	Output sample rate [samples per second]
$f_{\mathrm{Ch,BW}}$	$\mathbb{R}$	5G NR or LTE channel bandwidth [Hz]
B_m	$\mathbb{N}$	Number of OFDM symbols
$N_{\mathrm{CP},m,n}$	$\mathbb{N}$	High-rate CP length in samples
$N_{\mathrm{OFDM},m,n}$	$\mathbb{N}$	High-rate OFDM transform size
$f_{\mathrm{SCS},m,n}$	$\mathbb{R}$	OFDM subcarrier spacing [Hz]
$L_{\mathrm{act},m,n}$	$\mathbb{N}$	Number of active subcarriers
$\mu_{m,n}$	$\mathbb{N}$	OFDM subcarrier spacing scaling factor

in frequency range 1 (FR1). Without loss of generality, we assume that the number of samples to be processed is multiple of

$$N_{\mathrm{HSF}}^{\mathrm{samp}} = 0.5 \times 10^{-3} f_{\mathrm{s}}, \tag{1}$$

i.e., number of samples per half subframe corresponding to seven CP-OFDM symbols with 15 kHz baseline SCS. The OFDM transform size can be determined as a ratio of sample rate and SCS as

$$N_{\mathrm{OFDM}} = \frac{f_{\mathrm{s}}}{f_{\mathrm{SCS}}} = \frac{f_{\mathrm{s}}}{2^{\mu} \times 15\,\mathrm{kHz}}. \tag{2}$$

The normal CP length for the nth symbol is determined in samples as

$$N_{\mathrm{CP},n} = \begin{cases} \dfrac{9}{128} N_{\mathrm{OFDM}} + \alpha, & \text{for } \mathrm{mod}\left(n, \dfrac{1}{2} N_{\mathrm{subframe}}^{\mathrm{symb}}\right) = 0 \\ \dfrac{9}{128} N_{\mathrm{OFDM}}, & \text{otherwise,} \end{cases} \tag{3a}$$

where

$$\alpha = \mathrm{mod}\left(N_{\mathrm{HSF}}^{\mathrm{samp}}, 9 + 128\right) \tag{3b}$$

and $N_{\mathrm{subframe}}^{\mathrm{symb}} = N_{\mathrm{slot}}^{\mathrm{symb}} N_{\mathrm{subframe}}^{\mathrm{slot}}$ is the number of symbols per subframe. In 5G-NR numerology (as well as in LTE), longer CP for the first symbol is needed for each half subframe to balance the excess samples such that

$$\frac{1}{2} N_{\mathrm{subframe}}^{\mathrm{symb}} N_{\mathrm{OFDM},n} + \sum_{n=0}^{\frac{1}{2} N_{\mathrm{subframe}}^{\mathrm{symb}} - 1} N_{\mathrm{CP},n} = N_{\mathrm{HSF}}^{\mathrm{samp}}.$$

For the approaches proposed in this paper, *the SCS for each CP-OFDM symbol on each subband can be independently adjusted.* Therefore, we denote the SCS for the nth symbol on the mth subband by $f_{\mathrm{SCS},m,n}$ for $n \in \{0, 1, \ldots, B_m - 1\}$ and $m \in \{0, 1, \ldots, M-1\}$, where B_m and M are the number of CP-OFDM symbols on subband m and number of subbands, respectively. Here, $f_{\mathrm{SCS},m,n}$ can be selected as $2^{\mu} \times 15$ kHz for $\mu = 0, 1, \ldots, 4$ and the SCS scaling factor of nth symbol on subband m is denoted by $\mu_{m,n}$. The notations used for denoting the numerology are summarized in Table III.

The following processing model supports mixed SCSs and allocation bandwidths. Therefore, we denote by $L_{\mathrm{act},m,n}$, the number of active subcarriers of the nth symbol on subband m and $\mathcal{S}_{m,v} \subset \{0, 1, \ldots, B_m - 1\}$ for $v = 0, 1, \ldots, \Upsilon_m - 1$ is the set of symbol indices having the same symbol length and the same number of active subcarriers while Υ_m is the number of symbol sets with different numerology on subband m. Here, the number of active subcarriers can be selected as $L_{\mathrm{act},m,n} \leq 12 \times N_{\mathrm{PRB,max}}$, where $N_{\mathrm{PRB,max}}$ is the corresponding transmission bandwidth configuration defining the maximum number of active physical resource blocks (PRBs) given in [25, Table 5.3.2-1] for FR1.

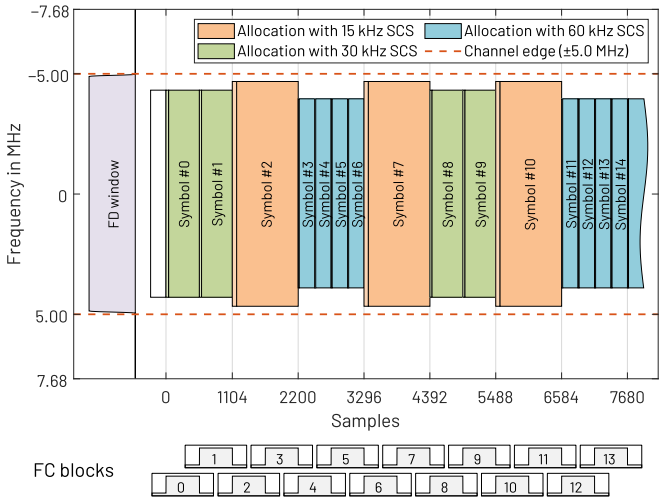

Fig. 2. Time-multiplexed mixed-numerology scenario with three SCSs. In this example, $\mathcal{S}_{0,0} = \{2, 7, 10\}$ is the set of symbol indices with 15 kHz SCS, $\mathcal{S}_{0,1} = \{0, 1, 8, 9\}$ are the indices for symbols with 30 kHz SCS, and $\mathcal{S}_{0,2} = \{3, 4, 5, 6, 11, 12, 13, 14\}$ for 60 kHz SCS. The number of active subcarriers in 10 MHz channel for symbols with 15 kHz, 30 kHz, and 60 kHz SCSs are 624, 288, and 132, respectively [20].

Fig. 2 illustrates a single subchannel ($M = 1$) time-multiplexed mixed-numerology scenario with three ($\Upsilon_0 = 3$) SCSs. In this example, $\mathcal{S}_{0,0} = \{2, 7, 10\}$ is the set of symbol indices with 15 kHz SCS while $\mathcal{S}_{0,1} = \{0, 1, 8, 9\}$ and $\mathcal{S}_{0,2} = \{3, 4, 5, 6, 11, 12, 13, 14\}$ are the indices for symbols with 30 kHz and 60 kHz SCS, respectively. In this scenario, we consider 10 MHz 5G-NR channel, where OFDM transform sizes are $N_{\mathrm{OFDM},m,n} = 1024$ for $n \in \mathcal{S}_{0,0}$, $N_{\mathrm{OFDM},m,n} = 512$ for $n \in \mathcal{S}_{0,1}$, and $N_{\mathrm{OFDM},m,n} = 256$ for $n \in \mathcal{S}_{0,2}$ while the corresponding number of active subcarriers are $L_{\mathrm{act},m,n} = 12 \times 52 = 624$, $L_{\mathrm{act},m,n} = 12 \times 24 = 288$, and $L_{\mathrm{act},m,n} = 12 \times 11 = 132$, respectively. The sampling rate is $f_{\mathrm{s}} = 15.36$ MHz corresponding to $N_{\mathrm{HSF}}^{\mathrm{samp}} = 7680$ samples within the half subframe.

III. PROPOSED SYMBOLS-SYNCHRONOUS FC-BASED FILTERED-OFDM

In original FC-based filtered-OFDM (FC-F-OFDM), filtering is applied at subband level, utilizing normal CP-OFDM waveform with the same SCS over the fixed bandwidth [10], [12], [13], [16], [26]. In this approach, the filtering can be configured in time direction only with the granularity of half a subframe, corresponding to 7, 14, or 28 symbols with 15 kHz, 30 kHz, or 60 kHz SCSs, respectively. In the proposed model, each subband may have dynamic mixed numerology, that

is, SCS and/or number of active PRBs may change from one OFDM symbol to another. Let us denote by $\mathbf{y}_m$ the CP-OFDM waveform on subband m for $m = 0, 1, \ldots, M-1$, where M is the number of subbands. For the proposed scheme, these waveforms are constructed by concatenating B_m time-domain CP-OFDM symbols. Here, nth symbol for $n = 0, 1, \ldots, B_m - 1$ on subband m is first generated with the inverse fast Fourier transform (IFFT) of size $L_{\text{OFDM},m,n}$ from the frequency-domain data $\mathbf{x}_{m,n}$ with $L_{\text{act},m,n}$ active subcarriers. Then CP of length $L_{\text{CP},m,n}$ is inserted to each symbol.

FC-based filtered-OFDM schemes carry out the filtering in overlapped circular convolutions. Let us denote by $\mathbf{y}_{m,r}$ the rth overlapped block of size L_m of the mth waveform for $r = 0, 1, \ldots, R_m - 1$, where R_m is the number of blocks needed to process all the B_m OFDM symbols of the mth subband waveform. The TX processing of the rth block of the mth waveform can be expressed as

$$\mathbf{z}_{m,r} = \mathbf{F}_{m,r}\mathbf{y}_{m,r}, \tag{4}$$

where $\mathbf{F}_{m,r}$ is the synthesis convolution matrix of size $N \times L_m$ applied for the rth block and $\mathbf{z}_{m,r}$ is the resulting output block of size N. In general, the processing of (4) interpolates the samples of the input block by a factor of $I_m = N/L_m$. Therefore, the resulting OFDM symbol and CP lengths on the output side are $N_{\text{OFDM},m,n} = I_m L_{\text{OFDM},m,n}$ and $N_{\text{CP},m,n} = I_m L_{\text{CP},m,n}$, respectively. Output blocks $\mathbf{z}_{m,r}$ for $r = 0, 1, \ldots, R_m - 1$ on subband m are concatenated either using the OLS or OLA approach resulting to filtered-OFDM waveform $\mathbf{z}_m$. Finally, all the filtered subband waveforms $\mathbf{z}_m$ for $m = 0, 1, \ldots, M-1$ are summed to form a composite filtered-OFDM waveform.

FC bin spacing, i.e, the resolution of the FC processing, is determined as the ratio of output sample rate and FC inverse transform size as

$$f_{\text{BS}} = f_{\text{s}}/N. \tag{5}$$

FC bin spacing basically defines the frequency resolution of the FC-based filtering and this parameter can be selected independent of OFDM SCS.

Input block size L_m for the rth block on subband m is divided into the non-overlapping and overlapping part sizes, denoted by $L_{\text{S},m,r}$ and $L_{\text{O},m,r} = L_m - L_{\text{S},m,r}$, respectively. The overlapping part size is further divided into leading and tailing overlapping part sizes as $L_{\text{L},m,n} = \lceil L_{\text{O},m,n}/2 \rceil$ and $L_{\text{T},m,n} = L_m - L_{\text{L},m,n}$, respectively. The corresponding non-overlapping and overlapping part sizes on the high rate (output) side are denoted by $N_{\text{S},r}$ and $N_{\text{O},r}$, respectively. For the original schemes, the overlapping is fixed (e.g., 50%, i.e., $L_{\text{O},m,r} = L_{\text{S},m,r} = 0.5L_m$) and, as the block size is a power of two ($L_m = 2^n$) due to the efficient FFT realizations, the payload (non-overlapping) parts of the processing blocks are not synchronized with CP-OFDM symbols with non-zero CP length as illustrated in Fig. 3.

A. Proposed Continuous Symbol-Synchronized FC Processing

Proposed continuous symbol-synchronized FC processing segments each stream of time-domain OFDM symbols

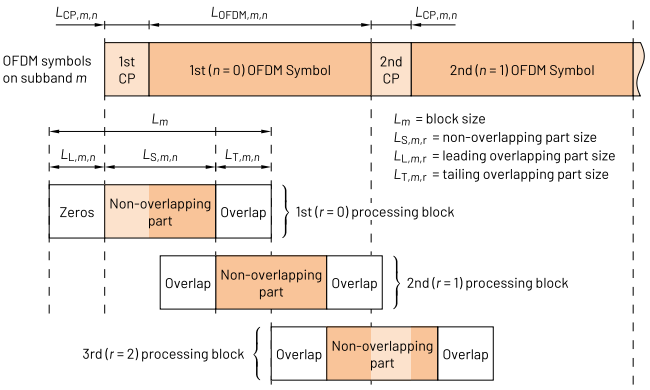

Fig. 3. FC block partitioning in basic continuous FC-F-OFDM. FC blocks are not synchronized to CP-OFDM symbols.

(corresponding to subband m) into overlapping processing blocks of size L_m as in earlier schemes. However, now the non-overlapping part of each processing block is aligned in time direction with the boundaries of the corresponding OFDM symbol. In addition, the overlap between the processing blocks is adjusted such that the size of the non-overlapping part for the FC blocks containing the CP part of the first symbol in a half subframe is longer than others. This segmentation of time-domain OFDM waveforms guarantees the processing of all numerologies of 5G NR and LTE synchronously as exemplified in Fig. 4.

Let us now represent the FC-based filtered-OFDM processing on subband m as

$$\mathbf{z}_m = \mathbf{F}_m \hat{\mathbf{y}}_m, \tag{6a}$$

where $\mathbf{F}_m$ is the block diagonal synthesis processing matrix of the form

$$\mathbf{F}_m = \text{bdiag}\left(\mathbf{F}_{m,0}, \mathbf{F}_{m,1}, \ldots, \mathbf{F}_{m,R_m-1}\right)_{q_{m,r},p_{m,r}} \tag{6b}$$

with overlapping blocks $\mathbf{F}_{m,r} \in \mathbb{C}^{N \times L_m}$ for $r = 0, 1, \ldots, R_m - 1$ and

$$\hat{\mathbf{y}}_m = \begin{bmatrix} \mathbf{0}_{L_{\text{L},m,0} \times 1} \\ \mathbf{y}_m \\ \mathbf{0}_{L_{\text{T},m,R_m-1} \times 1} \end{bmatrix} \tag{7}$$

is the time-domain CP-OFDM waveform with $L_{\text{L},m,0}$ and L_{T,m,R_m-1} samples zero padding before and after the CP-OFDM symbols, respectively.[1] This representation is equivalent with (4), however, more convenient from mathematical representation point of view. In (4), the waveform to be processed is segmented into overlapping blocks, that is, it models the realization of the processing. On the other hand, in (6), the synthesis matrix $\mathbf{F}_m$ is constructed using overlapped convolution matrices, i.e., this representation is used for modeling and analysis purposes. The notations used for denoting the FC processing parameters are summarized in IV.

[1]Here, $\text{bdiag}(\cdot)_{q_r,p_r}$ is an operator for constructing block-diagonal matrix with overlapping blocks of its arguments. The column and row indices of the first element of the rth block are q_r and p_r, respectively.

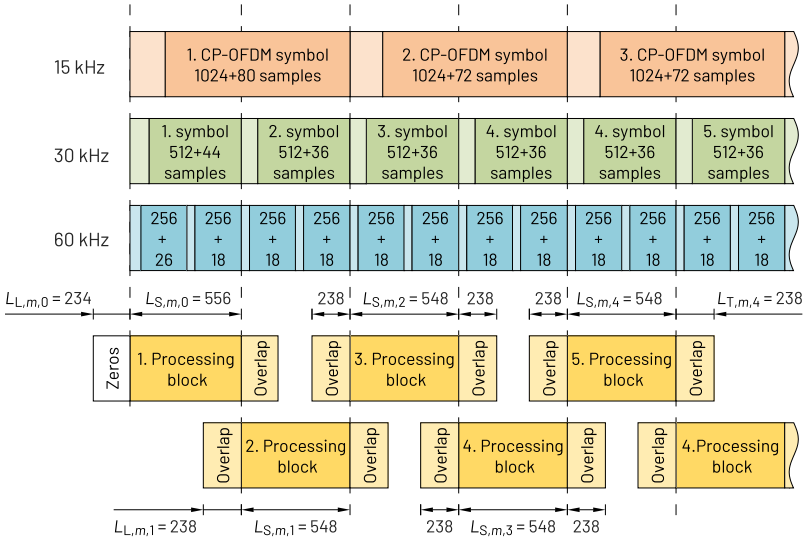

Fig. 4. Illustration of the block segmentation in proposed continuous symbol-synchronized FC processing. By adjusting the time locations of the FC processing blocks and the non-overlapping part size $L_{\mathrm{S},m,n}$, the FC blocks can be synchronized with all numerologies. For the first FC-processing block of each half subframe, the non-overlapping part size is larger.

TABLE IV

NOTATION USED FOR FC PROCESSING. SUBSCRIPT m DENOTES THE SUBBAND INDEX AND n DENOTES THE OFDM-SYMBOL INDEX

Notation	Dim.	Description
M	$\mathbb{N}$	Number of subbands
N	$\mathbb{N}$	FC processing IFFT size
L_m	$\mathbb{N}$	FC processing FFT size
I_m	$\mathbb{N}$	FC processing interpolation factor
R_m	$\mathbb{N}$	Number of FC processing blocks
$L_{\mathrm{CP},m,n}$	$\mathbb{N}$	Low-rate CP length in samples
$L_{\mathrm{OFDM},m,n}$	$\mathbb{N}$	Low-rate OFDM transform size
f_{BS}	$\mathbb{R}$	FC processing bin spacing [Hz]

Now, R_{HSF} denotes the number of half-subframes to be processed. For the proposed scheme, the non-overlapping part size for FC blocks for $r = 0, 1, \ldots, R_{\mathrm{HSF}}R_m - 1$ is given by

$$L_{\mathrm{S},m,r} = \begin{cases} 2^{\beta_m}(9+128)+\alpha, & \text{for } \mathrm{mod}(r, R_m) = 0 \\ 2^{\beta_m}(9+128), & \text{otherwise,} \end{cases} \tag{8a}$$

where

$$\beta_m = \left\lfloor \frac{1}{2}\frac{L_m}{128} \right\rfloor \tag{8b}$$

and α is given by (3b). Here, the number of FC-processing blocks within the half subframe is determined as

$$R_m = \begin{cases} 14 & \text{for 15 kHz FC bin spacing} \\ 28 & \text{for 30 kHz FC bin spacing} \\ 56 & \text{for 60 kHz FC bin spacing.} \end{cases} \tag{9}$$

For example, for 15 kHz FC-processing bin spacing in 10 MHz channel, as illustrated in Fig. 4, the input block length is $L_m = 1024$. In this case, the non-overlapping part size for the first FC block of each subframe is $L_{\mathrm{S},m,r} = 556$ samples whereas for the other FC blocks the corresponding number is $L_{\mathrm{S},m,r} = 548$ samples. In this case, exactly two FC-processing blocks are needed to process one, two, or four OFDM symbols with 15 kHz, 30 kHz, or 60 kHz SCS, respectively, as shown in Fig. 4. For $L_m = 512$, the corresponding number of FC-processing blocks is four, that is, the filtering can be reconfigured with the shortest (60 kHz SCS) OFDM symbol time resolution.

In representation of (6), the column and row indices of the first element of the rth block are q_r and p_r, respectively. In order to align the FC-processing blocks with CP-OFDM symbols, the row and column indices for the first elements of the rth block are given as

$$p_{m,r} = \begin{cases} rL_{\mathrm{S},m,n} + \dfrac{\alpha}{2}\left\lfloor \dfrac{r}{R_m} \right\rfloor, & \text{for } \mathrm{mod}(r, R_m) = 0 \\ rL_{\mathrm{S},m,n} + \dfrac{\alpha}{2}\left\lceil \dfrac{r}{R_m} \right\rceil, & \text{otherwise} \end{cases} \tag{10a}$$

and

$$q_{m,r} = I_m p_{m,r}, \tag{10b}$$

respectively. The resulting block diagonal structure of $\mathbf{F}_m$ with overlapping blocks is depicted in Fig. 5.

For efficient implementation, the processing realized by the convolution matrices of $\mathbf{F}_{m,r}$ in (4) or (6) may be decomposed as follows:

$$\mathbf{F}_{m,r} = \mathbf{S}_r \mathbf{W}_N^{\mathsf{H}} \mathbf{M}_{m,r} \mathbf{D}_{m,r} \mathbf{P}_{L_m} \mathbf{W}_{L_m} \mathbf{A}_{m,r}, \tag{11}$$

where $\mathbf{A}_{m,r} = \mathrm{diag}(\mathbf{a}_{m,r})$ and $\mathbf{S}_r = \mathrm{diag}(\mathbf{s}_r)$ are the time-domain analysis and synthesis windowing matrices with the analysis and synthesis window weights $\mathbf{a}_{m,r} \in \mathbb{R}^{L_m \times 1}$ and $\mathbf{s}_r \in \mathbb{R}^{N \times 1}$, respectively. $\mathbf{W}_{L_m} \in \mathbb{C}^{L_m \times L_m}$ and $\mathbf{W}_N^{\mathsf{H}} \in \mathbb{C}^{N \times N}$ are the unitary discrete Fourier transform (DFT) and inverse discrete Fourier transform (IDFT) matrices, respectively. $\mathbf{P}_{L_m} \in \mathbb{N}^{L_m \times L_m}$ is the FFT-shift matrix and

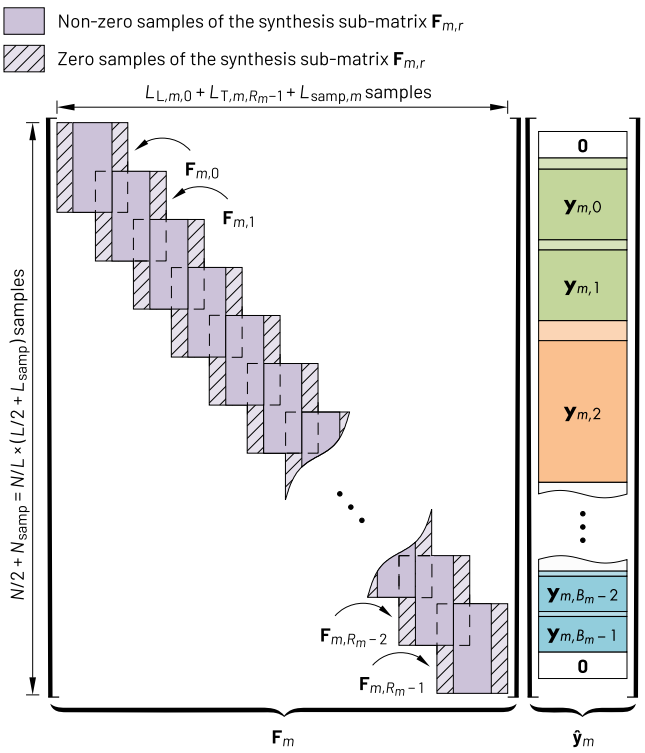

Fig. 5. Illustration of the structure of FC processing matrix $\mathbf{F}_m$ with R_m overlapping blocks.

$\mathbf{M}_{m,r} \in \mathbb{C}^{N \times L_m}$ maps L_m consecutive frequency-domain bins of the input signal to L_m consecutive frequency-domain bins of the output signal as well as the rotates the phases for maintaining the phase continuity. For OLA scheme, the analysis and synthesis time-domain windows are given as

$$\mathbf{a}_{m,r} = \begin{bmatrix} \mathbf{0}_{L_{\mathrm{L},m,r} \times 1} \\ \mathbf{1}_{L_{\mathrm{S},m,r} \times 1} \\ \mathbf{0}_{L_{\mathrm{T},m,r} \times 1} \end{bmatrix} \quad \text{and} \quad \mathbf{s}_r = \left[\mathbf{1}_{N \times 1}\right], \tag{12a}$$

respectively, whereas for OLS scheme these windows are given by

$$\mathbf{a}_{m,r} = \left[\mathbf{1}_{L_m \times 1}\right] \quad \text{and} \quad \mathbf{s}_r = \begin{bmatrix} \mathbf{0}_{N_{\mathrm{L},r} \times 1} \\ \mathbf{1}_{N_{\mathrm{S},r} \times 1} \\ \mathbf{0}_{N_{\mathrm{T},r} \times 1} \end{bmatrix}, \tag{12b}$$

respectively. Finally, the frequency-domain window for the rth block on subband m is determined by diagonal matrix $\mathbf{D}_{m,r}$. The formal definition for the frequency-domain windows for reducing the out-of-band emissions (OOBEs) and INI is given in Appendix. This appendix also describes how the frequency-domain windows can be used for realizing adjustable fractional delays using FC processing. The high-level block diagram of the proposed FC-based TX waveform processing for 5G NR following the decomposition of (11) is illustrated in Fig. 6. In this realization, the IFFTs of size N on the high-rate side have been combined.

By following the proposed segmentation of the subband waveforms into the overlapping FC blocks and then carrying out the overlapped circular convolutions with the aid of FC-based SFB (FFT/IFFT pair with windowing) in conjunction of OLA or OLS schemes, even the center frequency of each symbol may adjusted independently.

For FC-based filtered-OFDM, the corresponding time-domain CP-OFDM waveforms can be generated with lowest power-of-two transform size larger than $L_{\mathrm{act},m,n}$, i.e., $L_{\mathrm{OFDM},m,n} = 2^{\lceil \log_2(L_{\mathrm{act},m,n}) \rceil}$ and the FC processing interpolates the CP-OFDM waveform at the desired output rate. For continuous FC-processing alternatives (as opposite to [16]), the sampling-rate conversion factor has to be selected such that the CP length on the low-rate side is still an integer, i.e., the shortest OFDM transform size is $L_{\mathrm{OFDM,min}} = 128$ corresponding to CP length of $L_{\mathrm{CP,min}} = 9$ samples. Furthermore, the non-overlapping part size $L_{\mathrm{S},m,n}$ has also to be integer, restricting the L_m to be larger than equal to 256.

B. FC Filtered-OFDM RX Processing

FC-F-OFDM waveform can be received transparently, e.g., with *i)* basic CP-OFDM receiver, *ii)* by first filtering the received waveform, either using the FC-based analysis filter bank (AFB) or conventional time-domain filter, or *iii)* by using windowed overlap-and-add (WOLA) processing in connection with OFDM processing.

The FC-based AFB processing can be described as

$$\widetilde{\mathbf{y}}_m = \mathbf{G}_m \widetilde{\mathbf{z}}, \tag{13}$$

where the analysis processing matrix is $\mathbf{G}_m = \mathbf{F}_m^{\mathsf{H}}$ and $\widetilde{\mathbf{z}}$ is the received FC-F-OFDM waveform. Analogous to SFB case, the decimation factor D_m provided by the analysis processing is the ratio of long forward transform and short inverse transform sizes.

Finally, the filtered and possibly decimated subband signals $\widetilde{\mathbf{y}}_m$ for $m = 0, 1, \ldots, M-1$ are demodulated by using the conventional CP-OFDM RX processing as expressed by

$$\widetilde{\mathbf{x}}_m = \mathbf{Q}_m \widetilde{\mathbf{y}}_m, \tag{14a}$$

where

$$\mathbf{Q}_m = \mathrm{diag}\left(\mathbf{Q}_{m,0}, \mathbf{Q}_{m,1}, \ldots, \mathbf{Q}_{m,B_m-1}\right) \tag{14b}$$

with

$$\mathbf{Q}_{m,n} = \widehat{\mathbf{W}}_{m,n} \mathbf{R}_{N_{\mathrm{CP},m,n}}^{(\tau_{m,n})}. \tag{14c}$$

Here, $\widehat{\mathbf{W}}_{m,n}$ is the pruned unitary DFT matrix as given by

$$\left[\widehat{\mathbf{W}}_{m,n}\right]_{p,q} = \frac{1}{\sqrt{L_{\mathrm{OFDM},m,n}}} \exp\left(\frac{-\mathrm{j}\pi q\,(2p - L_{\mathrm{act},m,n})}{L_{\mathrm{OFDM},m,n}}\right) \tag{14d}$$

for $p = 0, 1, \ldots, L_{\mathrm{act},m,n} - 1$ and $q = 0, 1, \ldots, L_{\mathrm{OFDM},m,n} - 1$ and $\mathbf{R}_{m,n}^{(\tau_{m,n})} \in \mathbb{Z}^{L_{\mathrm{OFDM},m,n} \times (L_{\mathrm{OFDM},m,n} + L_{\mathrm{CP},m,n})}$ is the following CP removal matrix

$$\mathbf{R}_{m,n}^{(\tau_{m,n})} = \mathbf{C}_{L_{\mathrm{OFDM},m,n}}^{(-\tau_{m,n})} \begin{bmatrix} \mathbf{0}_{(L_{\mathrm{CP},m,n} - \tau_{m,n}) \times L_{\mathrm{OFDM},m,n}} \\ \mathbf{I}_{L_{\mathrm{OFDM},m,n}} \\ \mathbf{0}_{\tau_{m,n} \times L_{\mathrm{OFDM},m,n}} \end{bmatrix}^{\mathsf{T}}, \tag{14e}$$

where $\mathbf{C}_p^{(q)}$ is the circular shift matrix of size p used to shift the elements of a column vector downward by q elements.

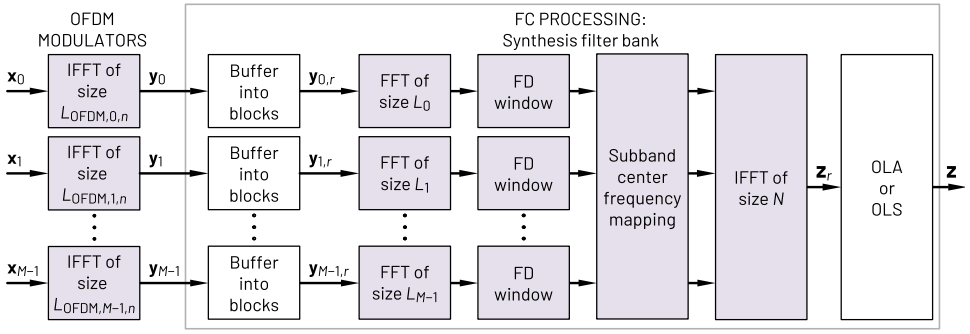

Fig. 6. Block diagram for the proposed transmitter processing using FC synthesis filter bank (SFB) with M subbands. In FC-based filtered-OFDM, filtering is applied at subband level, which means one or multiple contiguous PRBs with same SCS while different SCS may be utilized for different symbols within the subband. FC-processing consist of forward transforms of size L_m for $m = 0, 1, \ldots, M-1$ and inverse transform of size N. The center frequency of each symbol may be adjusted independently by simply mapping the corresponding frequency-domain bins.

Here, parameter $\tau_{m,n}$ is used to control the sampling instant within the CP-OFDM symbol as described in Section IV.

The realization of the FC processing on the RX side is similar to structure shown in Fig. 6 except that now the input waveform is buffered into overlapped blocks of size N. These blocks are converted into frequency domain, and L_m bins are selected from each subband. These bins are further windowed and converted back to time domain, and finally the time-domain blocks on each subband are concatenated using the OLA or OLS scheme.

The complexity of this scheme, in terms of multiplications, is the same as for symbol-synchronized discontinuous FC processing described in [16], i.e., 2–5 times the complexity of plain CP-OFDM. The channel estimation and equalization functionalities can be realized as for the conventional CP-OFDM waveform.

IV. Waveform Requirements and Metrics

In this paper, the performance of the FC-F-OFDM waveforms are evaluated with respect to requirements defined for the 5G-NR waveform in 3GPP specification for base stations [20]. The quality of the transmitted waveform is specified by the error vector magnitude (EVM) requirements, defining the maximum allowable deviation of the transmitted symbols with respect to ideal ones. The OOBE requirements, on the other hand, give the requirements for the tolerable spectral emissions of TX waveform. In addition to these two key metrics, there are other measures, e.g., adjacent channel selectivity (ACS), in-band blocking (IBB), out-of-band blocking (OOBB), among others, however, these measures are beyond the scope of this paper.

A. Error Vector Magnitude

The quality of the TX processing in 5G NR is measured by evaluating the mean-squared error (MSE) between the transmitted and ideal symbols. For the proposed approach, Υ_m symbol sets with different numerology are allowed on subband m and, therefore, the MSE is evaluated separately for each numerology as

$$\epsilon_{\mathrm{MSE},m,\upsilon} = \frac{1}{|\mathcal{S}_{m,\upsilon}|} \sum_{n \in \mathcal{S}_{m,\upsilon}} |\widetilde{\mathbf{x}}_{m,n} - \mathbf{x}_{m,n}|^2 \qquad (15)$$

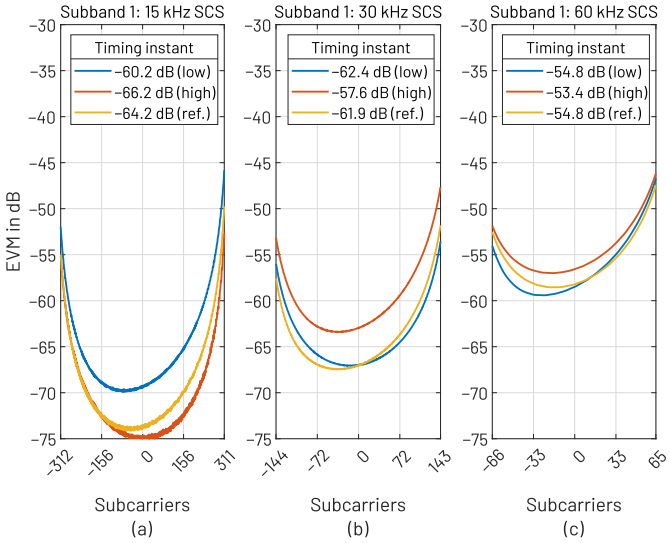

Fig. 7. EVMs for the example mixed-numerology scenario in Fig. 2. (a) 15 kHz SCS with 624 active SCs, (b) 30 kHz SCS with 288 active SCs, and (c) 60 kHz SCS with 132 active SCs. EVMs are evaluated with the reference timing (ref.) as well as $N_{\mathrm{EVM}}/2$ samples before (low) and after (high) the reference timing. 5G-NR EVM window values from [20, Tables B.5.2-1, B.5.2-2, and B.5.2-3] are used. The average EVMs over the active subcarriers are shown at the legend.

for $\upsilon = 0, 1, \ldots, \Upsilon_m - 1$ as illustrated in Fig. 7. The corresponding error vector magnitude (EVM) in percents is expressed as

$$\epsilon_{\mathrm{EVM},m,\upsilon} = 100\sqrt{\epsilon_{\mathrm{MSE},m,\upsilon}}. \qquad (16)$$

In this contribution, the EVM is expressed in decibels as

$$\epsilon_{\mathrm{EVM},m,\upsilon} = 10\log_{10}(\epsilon_{\mathrm{MSE},m,\upsilon}). \qquad (17)$$

Here, MSE and EVM are measured after executing zero-forcing equalizar (ZFE), as defined in [20, Annexture B].

The average MSE is defined as the arithmetic mean of the MSE values on active subcarriers, as given by

$$\bar{\epsilon}_{\mathrm{MSE},m,\upsilon} = \frac{1}{L_{\mathrm{act},\upsilon}} \mathbf{1}_{1\times L_{\mathrm{act},\upsilon}} \boldsymbol{\epsilon}_{\mathrm{MSE},m,\upsilon} \qquad (18)$$

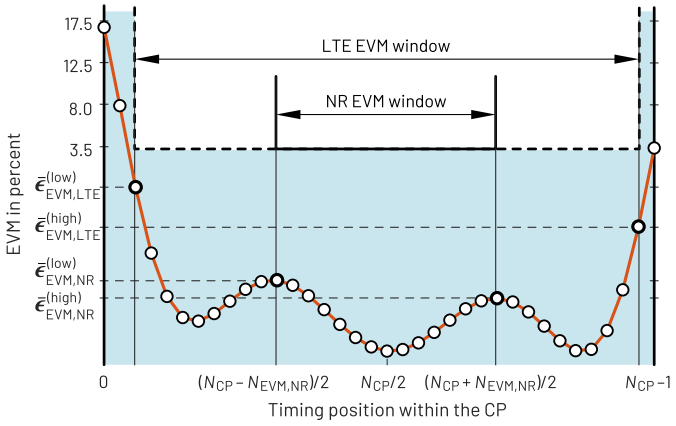

Fig. 8. EVM is measured at both sides of the ideal timing instance where the measurement positions are defined by the EVM window length. The LTE EVM window is considerably longer than the 5G-NR EVM window.

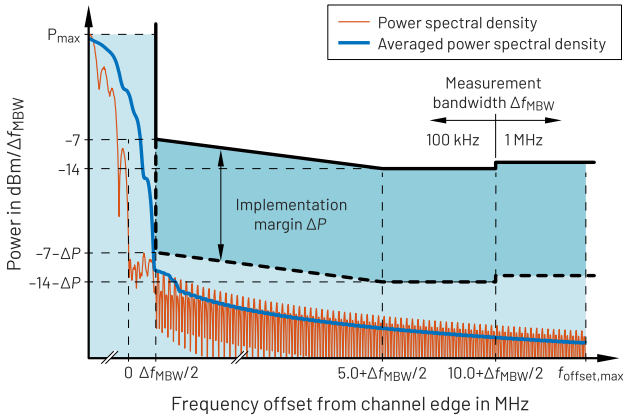

Fig. 9. Example PSDs and typical OBUE requirements (following [20, Table 6.6.4.2.1-2]). Here, the maximum PSD level $P_{\max}$ is determined based on the maximum output power of the base station.

Here, $L_{\text{act},\upsilon}$ is the number of active subcarriers for the symbols in index set $\mathcal{S}_{m,\upsilon}$, that is, $L_{\text{act},m,n}$ for $n \in \mathcal{S}_{m,\upsilon}$. The corresponding average EVM is denoted by $\bar{\epsilon}_{\text{EVM},m,\upsilon}$.

In general, EVM can be measured at $N_{\text{CP},m,n}$ timing instances by modifying the CP removal matrix as expressed by (14e). In this case, the timing adjustment has to be compensated by circularly shifting the OFDM symbols before taking the FFT. According to [20], the timing instant in the middle of the CP is selected as a reference point and the EVM performance before and after the reference point is measured in order to characterize the EVM performance degradation with respect to timing errors.

Fig. 8 illustrates the EVM evaluation for LTE and 5G-NR waveforms. In the case of 5G-NR waveform, the EVM is measured $N_{\text{EVM,NR}}/2$ samples before and after the reference point, where $N_{\text{EVM,NR}}$ is the EVM window length, and the corresponding EVM values are denoted as $\bar{\epsilon}^{(\text{low})}_{\text{EVM,NR}}$ and $\bar{\epsilon}^{(\text{high})}_{\text{EVM,NR}}$, respectively. The requirements for the EVM can be interpreted in the context of the EVM requirements of 5G NR, stated as $\{17.5\%, 12.5\%, 8.0\%, 3.5\%\}$ or $\{-15\,\text{dB}, -18\,\text{dB}, -22\,\text{dB}, -29\,\text{dB}\}$ for QPSK, 16-QAM, 64-QAM, 256-QAM, respectively [20, Table 6.5.2.2-1].

For LTE, $\bar{\epsilon}^{(\text{low})}_{\text{EVM,LTE}}$ and $\bar{\epsilon}^{(\text{high})}_{\text{EVM,LTE}}$ are evaluated in a same manner, however, while the 5G-NR EVM window lengths are 40–60% of the CP size [20, Tables B.5.2-1–B.5.2-3 for FR1], the corresponding LTE EVM windows are considerably longer, that is, 55.6–94.4% [25, Table E.5.1-1] implying relaxed time-synchronization requirements although more stringent requirements for waveform purity.

B. Unwanted Emissions

In the base station case, out-of-band emissions (OOBEs) are unwanted emissions immediately outside the channel bandwidth. The OOBE requirements for the base station transmitter are specified both in terms of operating band unwanted emissions (OBUE) and adjacent channel leakage power ratio (ACLR). OBUE define all unwanted emissions in each supported downlink operating band as well as the frequency ranges Δf_{OBUE} above and Δf_{OBUE} below each band. In 5G NR, $\Delta f_{\text{OBUE}} = 10\,\text{MHz}$ in FR1 [20, Table 6.6.1-1]. ACLR is the ratio of the filtered mean power centred on the assigned channel frequency to the filtered mean power centred on an adjacent channel frequency [20].

Fig. 9 illustrates typical OBUE requirements adopting the limits defined in [20, Table 6.6.4.2.1-2]. Thin (red) response shows the non-averaged power spectral density (PSD) estimate and thick (blue) solid response shows the averaged PSD estimate with measurement bandwidth (MBW) of Δf_{MBW}. Now, the requirements are stated such that for frequency offset of $f_{\text{offset}} = \Delta f_{\text{MBW}}/2$ from the channel edge, the maximum allowed power for the averaged PSD estimate is $-7\,\text{dBm}$. This requirement increases linearly to $-14\,\text{dBm}$ for frequency offset of $f_{\text{offset}} = 5\,\text{MHz} + \Delta f_{\text{MBW}}/2$ and maintains a constant value until $f_{\text{offset}} = 10\,\text{MHz} + \Delta f_{\text{MBW}}/2$. The maximum carrier output power of the (wide-area) base station is vendor specific, e.g., $P_{\max} = 33\,\text{dBm}$ in 10 MHz channel, translating into 40 dB attenuation requirement at the channel edge with respect to in-band level for the waveform generation. In addition to these requirements, some additional margin is needed to cope with performance degradation due to implementation non-idealities, i.e., finite-precision arithmetic, power amplifier (PA) non-linearity, etc. Similarly, on the RX side, certain level of frequency selectivity is needed in order to limit the INI as well as to provide sufficient rejection from RF blockers and other interferences.

The PSD estimate (or *the sample spectrum*) of the transmitted waveform can be evaluated by taking the DFT of the time-domain waveform and then squaring the absolute value of the resulting frequency-domain response as given by [27]

$$\tilde{\mathbf{s}}_{\mathbf{z}} = \frac{1}{N_{\text{PSD}}} \left| \mathbf{W}_{N_{\text{PSD}}} \begin{bmatrix} \mathbf{z} \\ \mathbf{0}_{(N_{\text{PSD}}-N_{\text{samp}})\times 1} \end{bmatrix} \right|^2. \tag{19}$$

Here, the signal is first zero padded to desired (e.g., power-of-two) size N_{PSD} and $\mathbf{W}_{N_{\text{PSD}}}$ is the DFT matrix of size N_{PSD}. The resolution bandwidth (RBW) of the non-averaged PSD estimate is $\Delta_{\text{RBW}} = f_{\text{s}}/N_{\text{PSD}}$. The PSD estimate for a given MBW Δ_{MBW} can obtained by averaging neighboring $N_{\text{avg}} = \Delta_{\text{MBW}}/\Delta_{\text{RBW}}$ spectral estimates [28]. Moving-average filter

can be conveniently realized using frequency-domain element-wise multiplication as

$$\bar{\mathbf{s}}_{\mathbf{z}} = \mathbf{W}_{N_{\text{PSD}}}^{\text{H}} \left([\mathbf{W}_{N_{\text{PSD}}} \mathbf{r}] \odot [\mathbf{W}_{N_{\text{PSD}}} \tilde{\mathbf{s}}_{\mathbf{z}}] \right), \tag{20}$$

where $\odot$ denotes the element-wise multiplication and the rectangular moving-average filter kernel is given by

$$\mathbf{r} = \begin{bmatrix} \mathbf{1}_{\lceil N_{\text{avg}}/2 \rceil \times 1} \\ \mathbf{0}_{(N_{\text{PSD}} - N_{\text{avg}}) \times 1} \\ \mathbf{1}_{\lfloor N_{\text{avg}}/2 \rfloor \times 1} \end{bmatrix}. \tag{21}$$

Adopting the specifications in [20] and [25], the MBW of $\Delta_{\text{MBW}} = 100\,\text{kHz}$ is commonly used for 5G-NR bands below 1 GHz whereas for 5G-NR bands above 1 GHz, $\Delta_{\text{MBW}} = 1\,\text{MHz}$ is also used for large frequency offsets from measurement filter centre frequency.

V. Numerical Examples

The performance and the flexibility of the proposed processing is demonstrated in terms of three examples. In all examples, FC-based filtering is also used on the RX side prior to OFDM demodulation if not stated otherwise.

A. Wide-Band Carrier With Guard-Band IoT

In this example, we demonstrate the co-existence of 5G-NR wide-band carrier and fourth generation (4G)-based narrow-band (NB) internet-of-things (IoT) carriers in a same channel. Here, we consider 20 MHz channel with NB-IoT on the guard-band of the wide-band carrier. The wide-band carrier has $L_{\text{act},0,n} = 312$ active subcarrierss (SCs) with 30 kHz SCSs for $n = 0, 1, \ldots, 13$ while the NB-IoT carriers have $L_{\text{act},1,n} = L_{\text{act},2,n} = L_{\text{act},3,n} = L_{\text{act},4,n} = 12$ SCs with 15 kHz SCSs for $n = 0, 1, \ldots, 6$. In this case, each pair of NB-IoT carriers is filtered as a single subband such that the total number of subbands (and frequency-domain windows) is three. The guard band between the narrow-band carriers with 15 kHz SCS and wide-band carrier with 30 kHz SCS is 180 kHz. In this case, 64-QAM is used on the wide-band carrier and QPSK on NB-IoT carriers. The OFDM transform size are now $4L_{\text{OFDM},0,n} = L_{\text{OFDM},1,n} = L_{\text{OFDM},2,n} = 256$, that is, the IoT subcarriers are interpolated by eight while the FC-processing transform sizes are $N = 8L_0 = L_1 = L_2 = 256$. In this case, the OLS-based processing is used, that is, the model with analysis and synthesis windows of (12a) are used.

The PSD of the resulting FC-based filtered-OFDM waveform is shown in Fig. 10 and the EVMs for the subbands are shown in Fig. 11. The power level at channel edge is $A_s = -78.0\,\text{dB}$ and the simulated EVM values for the carriers are $\bar{\epsilon}_{\text{EVM},0,0} = -49.5\,\text{dB}$, $\bar{\epsilon}_{\text{EVM},1,0} = -48.4\,\text{dB}$, and $\bar{\epsilon}_{\text{EVM},2,0} = -41.5\,\text{dB}$. Here, the EVM values of each pair of NB-IoT carriers are combined for simplicity. The simulated EVM values are at least 25 dB above the requirements. The corresponding EVM low and high values are shown in Fig. 11.

In this static case, similar performance can be obtained by using any filtering-based approaches including time-domain filtering. However, the complexity of the time-domain approaches is considerably higher. For example, the IoT waveform generation at sample rate of 1.92 Msps (one IFFT of size 128), filtering (symmetric finite impulse response (FIR) filter of order $n_0 = 95$), interpolation by using half-band filter chain (four half-band filters of order $n_1 = n_2 = n_3 = n_4 = 6$), and modulation at the desired center frequency takes about 30000 real multiplications per OFDM symbol. The corresponding filter transients are 831 samples. For the proposed approach, only three additional FFTs of size 256 are needed per OFDM symbol requiring 1284 real multiplications each. On the other hand, the corresponding emission level for the WOLA-based TX is $A_s = -36.5\,\text{dB}$ while the simulated EVMs values for the BWPs when WOLA is used on TX and RX sides are $\bar{\epsilon}_{\text{EVM},0,0} = -25.1\,\text{dB}$, $\bar{\epsilon}_{\text{EVM},1,0} = -36.5\,\text{dB}$, and $\bar{\epsilon}_{\text{EVM},2,0} = -22.8\,\text{dB}$. Therefore, the performance of WOLA TX clearly is not sufficient. In this case, maximal WOLA extension of size $L_{\text{ext}} = L_{\text{CP},m,n}/4$ samples is used.

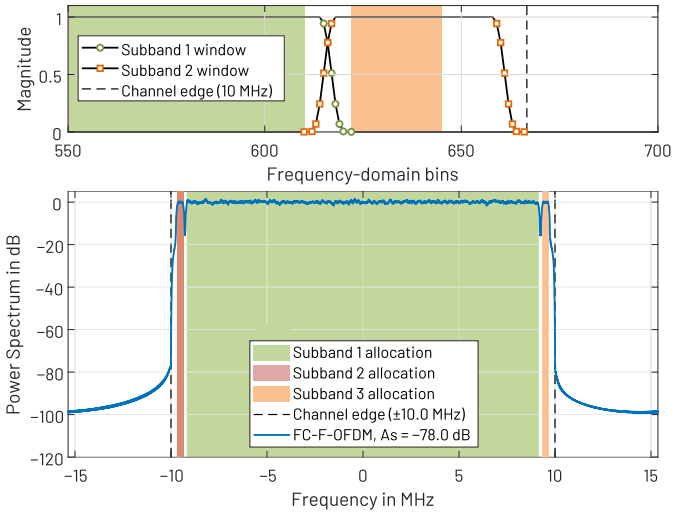

Fig. 10. PSD of the composite waveform and details of the frequency-domain windows in Example A.

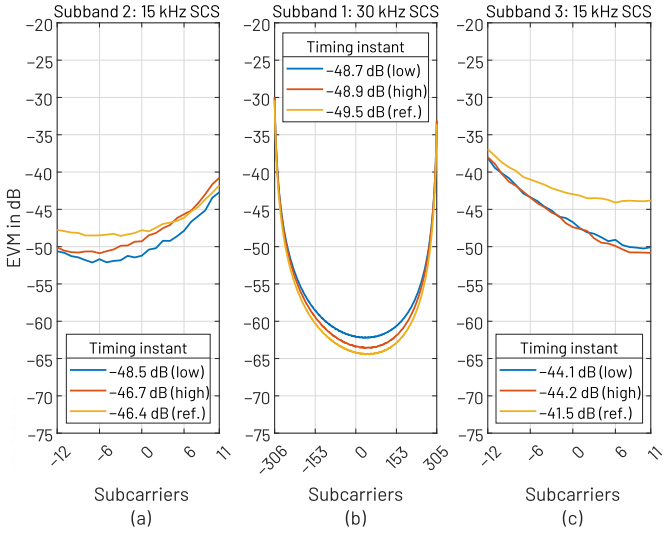

Fig. 11. EVM on each three subbands in Example A. (a) Leftmost subband containing two NB-IoT carriers with 15 kHz SCS. (a) 20 MHz carrier with 30 kHz SCS. (c) Rightmost subband containing two NB-IoT carriers with 15 kHz SCSs.

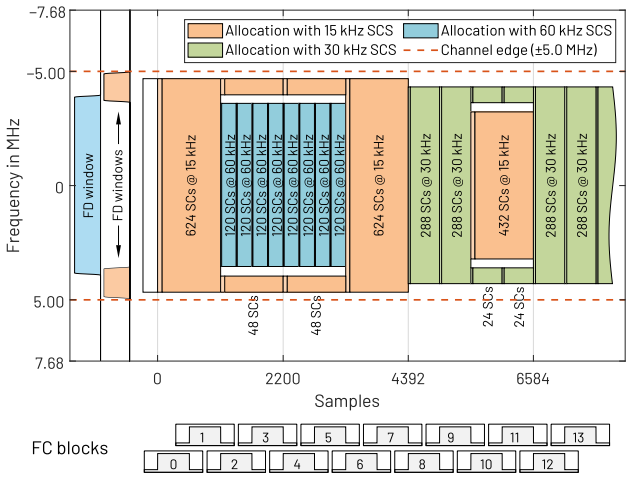

Fig. 12. Time-frequency allocation in Example B with mixed numerology. The frequency-domain windows during the rth FC block for $r = 2, 3, 4, 5$ are illustrated on the left hand side of the figure.

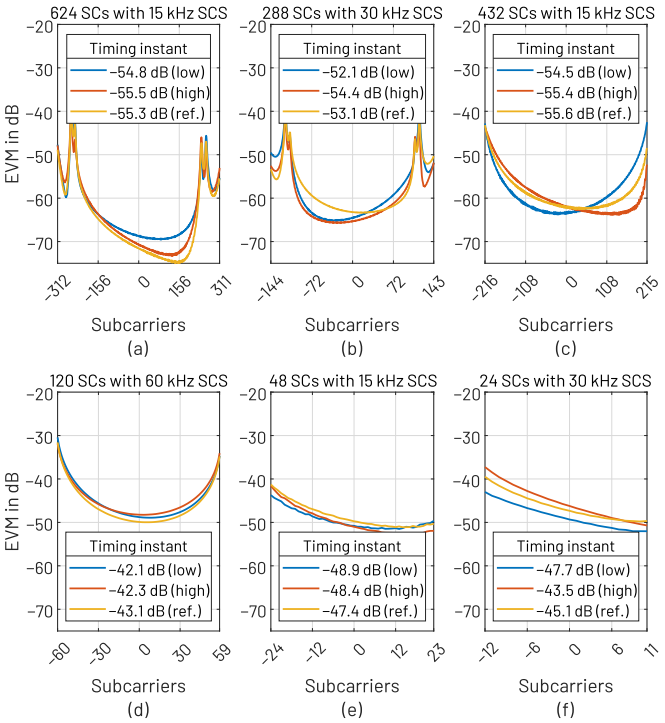

Fig. 13. EVM on each symbol in Example B. (a) 624 SCs with 15 kHz SCS. (b) 288 SCs with 30 kHz SCS. (c) 432 SCs with 15 kHz SCS. (d) 120 SCs with 60 kHz SCS. (e) 48 SCs with 15 kHz SCS. (f) 24 SCs with 30 kHz SCS.

B. SSB-Like Mixed-Numerology Scenario

In this example, we consider a synchronization signal block (SSB)-like scenario where a wide-band carrier with one SCS is punctured by the symbols with another SCS. In this case, four OFDM symbols with 15 kHz SCS ($L_{\text{act},0,n} = 624$ active SCs for $n = 0, 1, 2, 3$) and six symbols with 30 kHz SCS ($L_{\text{act},0,n} = 288$ active SCs for $n = 4, 5, \ldots, 9$) are transmitted in 10 MHz channel. Second and third symbol with 15 kHz SCS is punctured by the eight OFDM symbols with 60 kHz SCS (120 active SCs) such that the 528 innermost subcarriers of the symbols with 15 kHz SCS are deactivated. Third and fourth OFDM symbol with 30 kHz SCS is punctured by one OFDM symbol with 15 kHz SCS (432 active SCs) such that 240 SCs of the symbols with 30 kHz SCSs are deactivated. The resulting guard-band between the allocations with different SCSs is about 360 kHz. In this example, quadrature phase-shift keying (QPSK) is used for all allocations. The time-frequency allocation of this mixed-numerology scenario is detailed in Fig. 12. In the above, OLA-based processing is used.

The simulated power level at the channel edge is -76.9 dB. The EVMs for the symbols for each numerology are shown in Fig. 13. As seen, the symbols with 60 kHz SCSs have the worst EVM since, for these subcarriers, the guard-band relative to SCS is the smallest. The peaks seen in the EVM responses of Fig. 13(a) are due to the time-domain transients resulting from filtering the symbols with 60 kHz SCS. Similarly, the peaks in Fig. 13(b) are the transients of allocation with 432 SCs, i.e., the improved frequency-domain localization increases the dispersion in time domain, however, even with this inter-symbol interference (ISI), the EVM levels are still within the requirements.

Similar configuration cannot be realized with original FC processing as for these schemes the non-overlapping part size is always power of two (if effective power-of-two transform sizes are used) and, consequently, the FC processing blocks are divided equidistantly in time (not aligning with OFDM symbols with non-zero CP size). For time-domain approaches, different filters are needed for each bandwidth, that is, for subbands with 624, 120, 48, 288, 432, and 24 active SCs different filter needs to be applied. This would make the overall implementation overly complicated both in terms of computational complexity and filter coefficients to be stored. Furthermore, aligning the symbols in time direction needs special care as the delays of the filters are typically different.

C. Adjustable BWPs

In this example, we demonstrate the flexibility of the proposed scheme in the case where FC-based filtering is reconfigured for each symbol. In this case, we have two variable subbands: First subband has 15 kHz SCS and $L_{\text{act},0,n} = 192$ active SCs for $n = 0, 1, \ldots, 6$ while second has 30 kHz SCS and $L_{\text{act},1,n} = 72$ active SCs for $n = 0, 1, \ldots, 13$. The center frequency of the first subband is adjusted as $f_{0,n}^{(\text{center})} = 64(n-3) \times 15\,\text{kHz}$ for $n = 0, 1, \ldots, 6$ and the center frequency of the second subband is $f_{1,n}^{(\text{center})} = 218 \times 15\,\text{kHz}$ for $n = 0, 1, \ldots, 6$ and $f_{1,n}^{(\text{center})} = -218 \times 15\,\text{kHz}$ for $n = 7, 8, \ldots, 13$. This configuration is depicted in Fig. 14.

The PSD of resulting FC-based filtered-OFDM waveform is shown in Fig. 15 while the corresponding EVMs are shown in Fig. 16. As seen from these figures, the performance of the proposed scheme meets the requirements even at this most challenging scenario.

The presented solution allows unseen flexibility in supporting changing allocations in mixed-numerology scenarios with OFDM symbol resolution. This allows to support all envisioned use cases for 5G NR and provides a flexible starting point for sixth generation (6G) development.

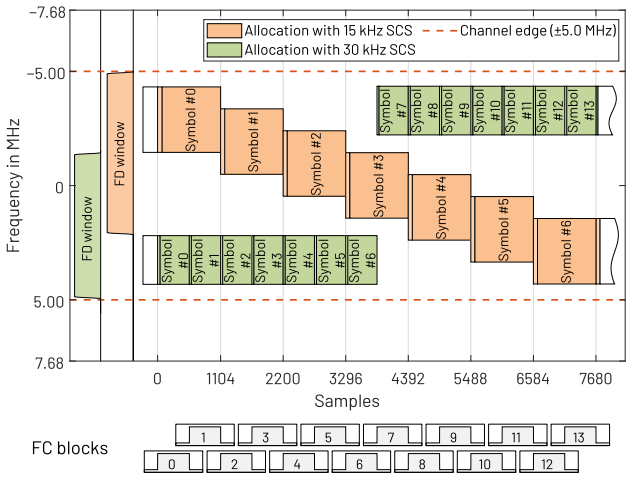

Fig. 14. Time-frequency allocation in Example C with two variable subbands. The frequency-domain windows during the two first FC blocks (first symbol with 15 kHz SCS and two first symbols with 30 kHz SCS) are illustrated on the left hand side of the figure.

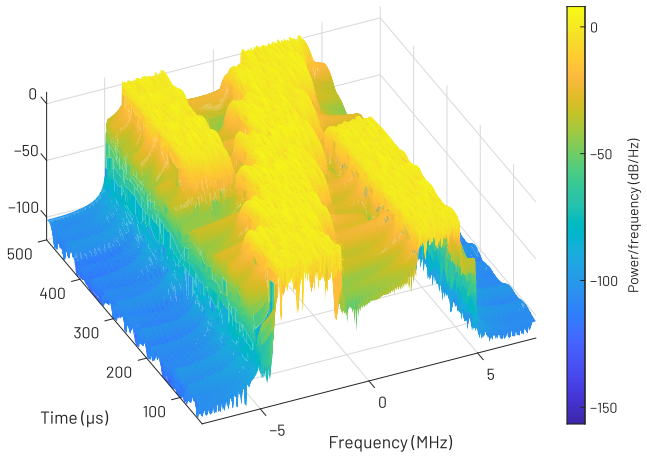

Fig. 15. PSD in Example C with two variable subbands.

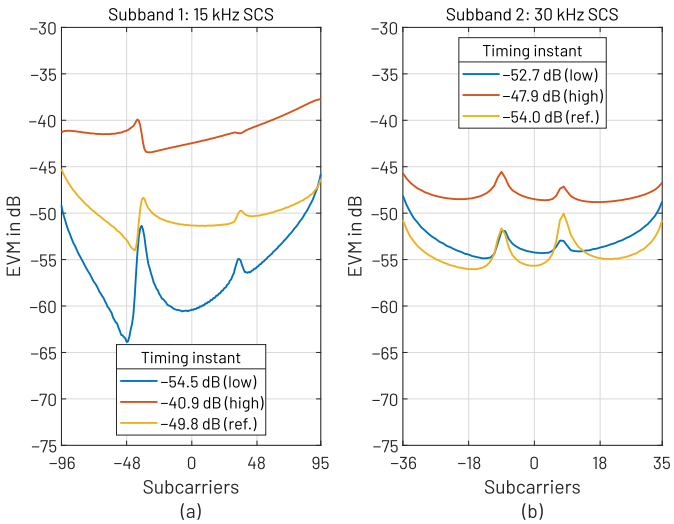

Fig. 16. EVM on each of two subbands in Example C. (a) BWP with 15 kHz SCS and 192 active SCs. (b) BWP with 30 kHz SCS and 72 active SCs.

VI. Conclusion

In this article, continuous symbol-synchronized fast-convolution (FC)-processing scheme was proposed, with particular emphasis on the physical-layer processing in fifth-generation new radio (5G NR) and beyond mobile radio networks. The proposed scheme was shown to offer various benefits over the basic continuous and discontinuous processing models, especially in providing excellent performance in reducing the unwanted emissions and inter-numerology interference in 5G-NR mixed-numerology scenarios while keeping in-band interference level well below the requirements stated in 3GPP specifications. Both dynamic and static filtering configurations are supported for all numerologies simultaneously providing greatly improved flexibility over the FC-processing schemes proposed earlier. The benefits are particularly important in specific application scenarios, like transmission of single or multiple narrow subbands, or in mini-slot type transmission, which is a core element in the ultra-reliable low-latency transmission service of 5G-NR networks.

Proposed scheme also provides lower complexity when compared to time-domain filtering-based approaches due to the efficient realization using FC. In addition, the resulting implementations for the filtered-OFDM waveform generation and the corresponding receiver side processing are highly modular, even with multiple subbands of different bandwidths, as the basic building blocks are only (I)FFTs and windowing with the same fixed set of transition-band weights. Furthermore, this scheme processes the symbols in block-wise manner and, therefore, long filter transients exceeding the symbol boundaries can be avoided.

It was shown through concrete numerical examples that only 180 kHz guard band is sufficient to support the co-existence of 5G-NR wide-band carrier with 30 kHz SCS and 4G-based NB-IoT carriers in a same channel. The simulated EVM values in this case are at least 25 dB above the fifth-generation new radio requirements while the margin to 3GPP spectral emission mask (SEM) is about 40.0 dB. For SSB-like scenarios, i.e., when the wide-band carrier with certain SCS is punctured by the allocation with another SCS, 360 kHz guard is sufficient both between the allocations with 15 kHz and 30 kHz SCS and allocations with 15 kHz and 60 kHz SCS. Similar EVM and OOBEs performances can be obtained in this case. The time dispersion introduced by the improved spectral confinement, may temporarily degrade the performance when the configuration is dynamically adjusted. However, these degradations are negligible with respect to requirements. The same level of flexibility and performance cannot be achieved with reasonable complexity by any other processing method, including the earlier FC processing solutions. These observations can be used as a basis for the next generation new radio (NR) standards.

This paper focused on enhanced FC processing in case of LTE and 5G-NR numerologies. Naturally, the proposed scheme can be adapted to other OFDM numerologies as well. Actually, the specific choices of CP length in LTE and 5G-NR introduce some additional complexity to FC processing in these systems, which could be avoided if the numerology is selected considering FC-based TX and RX signal processing.

Appendix

The frequency-domain characteristics of the FC processing are determined by the frequency-domain window. Basically, the frequency-domain window can be adjusted at the

granularity of FC bin spacing, as given by (5). For the proposed and the earlier approaches, the frequency-domain window consist of ones on the passband, zeros on the stopband, and two symmetric transition bands with $N_{\text{TB},m,n}$ nontrivial optimized prototype transition-band values. The same optimized transition band weights can be used for realizing all the transmission bandwidths by properly adjusting the number of one-valued weights between the transition bands.

According to [25, Table 5.3.3-1], the minimum guard bands for base station channel bandwidths are determined as

$$f_{\text{GB}} = \frac{1}{2}\left[f_{\text{BW}} - f_{\text{SCS}}(L_{\text{act,max}} + 1)\right], \tag{22}$$

where $L_{\text{act,max}} = 12 \times N_{\text{PRB,max}}$ with $N_{\text{PRB,max}}$ being the transmission bandwidth configuration. For example, in 10 MHz channel with 15 kHz SCS, the maximum number of active PRBs is $N_{\text{PRB,max}} = 52$ ($L_{\text{act,max}} = 624$) and the resulting guard band is $f_{\text{GB}} = 312.5$ kHz. Assuming FC bin spacing of $f_{\text{BS}} = 15$ kHz, i.e., $N = N_{\text{OFDM}} = 1024$, the guard band corresponds to the $f_{\text{GB}}/f_{\text{BS}} = 20.83$ frequency-domain bins. Now, the frequency-domain window can be determined such that 624 frequency-domain window values corresponding to active subcarriers are equal to one, $\lfloor 20.83 \rfloor = 20$ window values on both sides of the active subcarriers can be optimized for achieving the desired spectral characteristics while the remaining frequency-domain window values are equal to zero. Same frequency-domain window can be used for filtering the higher SCSs as well, since for given channel bandwidth the guard band increases as the SCS increases.

Let us denote the desired center frequency of each OFDM symbol by $f_{m,n}^{(\text{center})}$. The lower and higher passband (PB) edge frequencies of each symbol can then be expressed as

$$f_{\text{PB},m,n}^{(\text{low})} = f_{m,n}^{(\text{center})} - f_{\text{s}}\frac{L_{\text{act},m,n}/2}{L_{\text{OFDM},m,n}} \tag{23a}$$

and

$$f_{\text{PB},m,n}^{(\text{high})} = f_{m,n}^{(\text{center})} + f_{\text{s}}\frac{L_{\text{act},m,n}/2-1}{L_{\text{OFDM},m,n}}, \tag{23b}$$

respectively. Let us assume for simplicity that the center frequency of each subband is fixed and the subbands are sorted based on their center frequencies such that subband m for $m = 0$ has the lowest center frequency, subband m for $m = 1$ has the next lowest center frequency, and so on. Now, the stopband (SB) edge frequencies for the subbands can be expressed in the following three cases:

1) One Subband ($M = 1$): In this case, the stopband edges are determined based on the channel edges, that is, the lower and upper stopband edge frequencies are determined as

$$f_{\text{SB},0,n}^{(\text{low})} = -f_{\text{BW}}/2 \tag{24a}$$

and

$$f_{\text{SB},0,n}^{(\text{high})} = f_{\text{BW}}/2, \tag{24b}$$

respectively.

2) Two Subbands ($M = 2$): In this case, the lower (higher) stopband edge of the first (second) subband is determined by channel bandwidth while the higher (lower) stopband edge of the first (second) subband is determined by lower (higher) passband edge of the second (first) subband, that is, the lower and higher stopband edge frequencies are determined as

$$f_{\text{SB},m,n}^{(\text{low})} = \begin{cases} -f_{\text{BW}}/2 & \text{for } m = 0 \\ f_{\text{PB},0,n}^{(\text{high})} & \text{for } m = 1 \end{cases} \tag{25a}$$

and

$$f_{\text{SB},m,n}^{(\text{high})} = \begin{cases} f_{\text{PB},1,n}^{(\text{low})} & \text{for } m = 0 \\ f_{\text{BW}}/2 & \text{for } m = 1. \end{cases} \tag{25b}$$

3) Three or More Subbands ($M \geq 3$): Now, the lower and higher stopband edges are determined by

$$f_{\text{SB},m,n}^{(\text{low})} = \begin{cases} -f_{\text{BW}}/2 & \text{for } m = 0 \\ f_{\text{PB},m-1,n}^{(\text{high})} & \text{for } m = 1, 2, \ldots, M-2 \\ f_{\text{PB},M-2,n}^{(\text{high})} & \text{for } m = M-1 \end{cases} \tag{26a}$$

and

$$f_{\text{SB},m,n}^{(\text{high})} = \begin{cases} f_{\text{PB},1,n}^{(\text{low})} & \text{for } m = 0 \\ f_{\text{PB},m+1,n}^{(\text{low})} & \text{for } m = 1, 2, \ldots, M-2 \\ f_{\text{BW}}/2 & \text{for } m = M-1, \end{cases} \tag{26b}$$

that is, the upper (lower) stopband edge of the mth subband is determined by the $(m+1)$th ($(m-1)$th) subband except for the edgemost subbands, where the channel edge specifies the upper (lower) stopband edge of the last (first) subband.

The frequency-domain window for rth FC block on subband m is determined as

$$\mathbf{d}_{m,r} = \begin{bmatrix} \mathbf{0}_{k_{m,n}^{(\text{low})} \times 1} \\ \mathbf{h}_{m,n} \\ \mathbf{1}_{(k_{m,n}^{(\text{high})} - k_{m,n}^{(\text{low})} + 1 - 2N_{\text{TB},m,n}) \times 1} \\ \mathbf{J}_{N_{\text{TB},m,n}} \mathbf{h}_{m,n} \\ \mathbf{0}_{(L_m - 1 - k_{m,n}^{(\text{high})}) \times 1} \end{bmatrix}, \tag{27}$$

where $n \in \{0, 1, \ldots, B_{\text{OFDM},m} - 1\}$ is now the index of the symbol processed by the rth FC block. Here, $\mathbf{h}_{m,n} \in \mathbb{R}^{N_{\text{TB},m,n} \times 1}$ is the transition-band weight vector and $\mathbf{J}_{N_{\text{TB},m,n}}$ is the reverse identity matrix of size $N_{\text{TB},m,n}$ essentially reversing the order of transition-band weight vector. The lower and higher stopband indices of each subband in (27) are determined as

$$k_{m,n}^{(\text{low})} = \max\left(\left\lceil \left(f_{\text{SB},m,n}^{(\text{low})} - f_{m,n}^{(\text{center})}\right) N/f_{\text{s}} \right\rceil + L_m/2, 0\right) \tag{28a}$$

and

$$k_{m,n}^{(\text{high})} = \min\left(\left\lfloor \left(f_{\text{SB},m,n}^{(\text{high})} - f_{m,n}^{(\text{center})}\right) N/f_{\text{s}} \right\rfloor + L_m/2, L_m - 1\right), \tag{28b}$$

respectively.

For channelization purposes, the frequency-domain window values are real. FC processing can also be used for shifting the output of each subband by adjustable delay if needed. In this case, an additional phase term as given by

$$[\mathbf{d}_{m,r}]_q = \exp\left(-2\text{j}\pi(q - L_m/2)\Phi_{\text{FD},m}/L_m\right) \tag{29}$$

for $q = 0, 1, \ldots, L_m - 1$ is included in the coefficients. Here, $\Phi_{\text{FD},m} \in [0, 1]$ is the desired fractional delay value

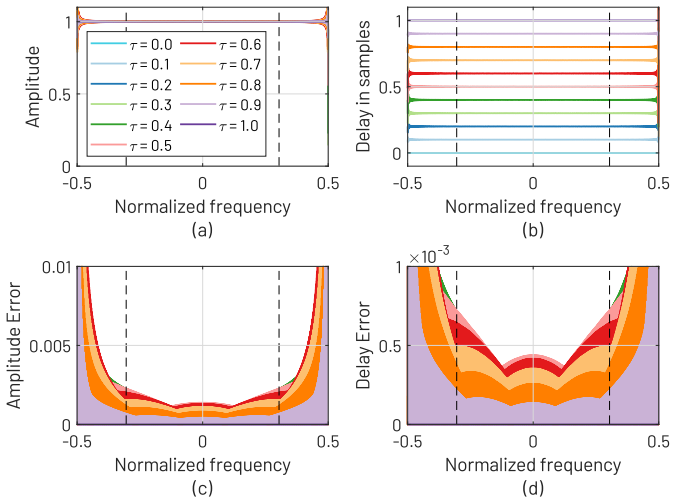

Fig. 17. Typical (a) amplitude and (b) delay responses for the FC-based fractional delay filter for $\Phi_{\mathrm{FD},m} \in \{0.0, 0.1, \ldots, 1.0\}$ as well as the corresponding (c) amplitude and (d) delay errors. The frequency range between the dashed lines corresponds to the transmission bandwidth.

on subband m. The characteristic responses for the FC-based fractional delay filter are illustrated in Fig. 17. Furthermore, the frequency-domain window weights can be used for realizing highly accurate equalizers, e.g., pre-compensating the amplitude and group-delay variations of the analog RF radio parts.

REFERENCES

[1] E. Dahlman, S. Parkvall, and J. Sköld, *5G NR: The Next Generation Wireless Access Technology*. New York, NY, USA: Academic, 2018.

[2] G. Wunder *et al.*, "5GNOW: Non-orthogonal, asynchronous waveforms for future mobile applications," *IEEE Commun. Mag.*, vol. 52, no. 2, pp. 97–105, Feb. 2014.

[3] P. Banelli, S. Buzzi, G. Colavolpe, A. Modenini, F. Rusek, and A. Ugolini, "Modulation formats and waveforms for 5G networks: Who will be the heir of OFDM?: An overview of alternative modulation schemes for improved spectral efficiency," *IEEE Signal Process. Mag.*, vol. 31, no. 6, pp. 80–93, Nov. 2014.

[4] J. Choi, B. Kim, K. Lee, and D. Hong, "A transceiver design for spectrum sharing in mixed numerology environments," *IEEE Trans. Wireless Commun.*, vol. 18, no. 5, pp. 2707–2721, May 2019.

[5] J. Mao, L. Zhang, P. Xiao, and K. Nikitopoulos, "Filtered OFDM: An insight into intrinsic in-band interference and filter frequency response selectivity," *IEEE Access*, vol. 8, pp. 100670–100683, 2020.

[6] E. Memisoglu, A. B. Kihero, E. Basar, and H. Arslan, "Guard band reduction for 5G and beyond multiple numerologies," *IEEE Commun. Lett.*, vol. 24, no. 3, pp. 644–647, Mar. 2020.

[7] M.-L. Boucheret, I. Mortensen, and H. Favaro, "Fast convolution filter banks for satellite payloads with on-board processing," *IEEE J. Sel. Areas Commun.*, vol. 17, no. 2, pp. 238–248, Feb. 1999.

[8] M. Borgerding, "Turning overlap-save into a multiband mixing, downsampling filter bank," *IEEE Signal Process. Mag.*, vol. 23, no. 2, pp. 158–161, Mar. 2006.

[9] M. Tanabe, M. Umehira, K. Ishihara, and Y. Takatori, "A new flexible channel access scheme using overlap FFT filter-bank for dynamic spectrum access," in *Proc. 15th Asia–Pacific Conf. Commun.*, Oct. 2009, pp. 178–181.

[10] M. Renfors, J. Yli-Kaakinen, T. Levanen, M. Valkama, T. Ihalainen, and J. Vihriala, "Efficient fast-convolution implementation of filtered CP-OFDM waveform processing for 5G," in *Proc. IEEE Globecom Workshops (GC Wkshps)*, San Diego, CA, USA, Dec. 2015, pp. 1–7, doi: 10.1109/GLOCOMW.2015.7414034.

[11] G. L. David, V. S. Sheeba, J. Chunkath, and K. R. Meera, "Performance analysis of fast convolution based FBMC-OQAM system," in *Proc. Int. Conf. Commun. Syst. Netw. (ComNet)*, Jul. 2016, pp. 65–70.

[12] J. Yli-Kaakinen *et al.*, "Efficient fast-convolution-based waveform processing for 5G physical layer," *IEEE J. Sel. Areas Commun.*, vol. 35, no. 6, pp. 1309–1326, Jun. 2017.

[13] J. Yli-Kaakinen, T. Levanen, M. Renfors, M. Valkama, and K. Pajukoski, "FFT-domain signal processing for spectrally-enhanced CP-OFDM waveforms in 5G new radio," in *Proc. 52nd Asilomar Conf. Signals, Syst., Comput.*, Oct. 2018, pp. 1049–1056, doi: 10.1109/ACSSC.2018.8645100.

[14] Y. Li, W. Wang, J. Wang, and X. Gao, "Fast-convolution multicarrier based frequency division multiple access," *Sci. China Inf. Sci.*, vol. 62, no. 8, Aug. 2019, 80301.

[15] A. Loulou, J. Yli-Kaakinen, and M. Renfors, "Advanced low-complexity multicarrier schemes using fast-convolution processing and circular convolution decomposition," *IEEE Trans. Signal Process.*, vol. 67, no. 9, pp. 2304–2319, May 2019, doi: 10.1109/TSP.2019.2904015.

[16] J. Yli-Kaakinen *et al.*, "Frequency-domain signal processing for spectrally-enhanced CP-OFDM waveforms in 5G new radio," *IEEE Trans. Wireless Commun.*, vol. 20, no. 10, pp. 6867–6883, Oct. 2021, doi: 10.1109/TWC.2021.3077762.

[17] M. Ishibashi, M. Umehira, X. Wang, and S. Takeda, "FFT-based frequency domain filter design for multichannel overlap-windowed-DFTs-OFDM signals," in *Proc. IEEE 93rd Veh. Technol. Conf. (VTC-Spring)*, Apr. 2021, pp. 1–5.

[18] X. Lin, L. Mei, F. Labeau, X. Sha, and X. Fang, "Efficient fast-convolution based hybrid carrier system," *IEEE Trans. Wireless Commun.*, vol. 21, no. 5, pp. 3508–3522, May 2022.

[19] M. Renfors, J. Yli-Kaakinen, and F. J. Harris, "Analysis and design of efficient and flexible fast-convolution based multirate filter banks," *IEEE Trans. Signal Process.*, vol. 62, no. 15, pp. 3768–3783, Aug. 2014, doi: 10.1109/TSP.2014.2330331.

[20] *Technical Specification Group Radio Access Network; NR; Base Station (BS) Radio Transmission and Reception (Release 16)*, document TS 38.104 V16.4.0, 3GPP, Jun. 2020.

[21] 3GPP, *5G; Study on New Radio (NR) Access Technology (Release 15)*, document TR 38.912 V15.0.0, Sep. 2019.

[22] J. Bazzi, K. Kusume, P. Weitkemper, K. Takeda, and A. Benjebbour, "Transparent spectral confinement approach for 5G," in *Proc. Eur. Conf. Netw. Commun. (EuCNC)*, Oulu, Finland, Jun. 2017, pp. 1–5.

[23] R. Zayani, H. Shaiek, X. Cheng, X. Fu, C. Alexandre, and D. Roviras, "Experimental testbed of post-OFDM waveforms toward future wireless networks," *IEEE Access*, vol. 6, pp. 67665–67680, 2018.

[24] T. Levanen, J. Pirskanen, K. Pajukoski, M. Renfors, and M. Valkama, "Transparent Tx and Rx waveform processing for 5G new radio mobile communications," *IEEE Wireless Commun.*, vol. 26, no. 1, pp. 128–136, Feb. 2019.

[25] *Technical Specification Group Radio Access Network; Evolved Universal Terrestrial Radio Access (E-UTRA); Base Station (BS) Radio Transmission and Reception (Release 16)*, document TS 36.104 V16.6.0, 3GPP, Jun. 2020.

[26] M. Renfors, J. Yli-Kaakinen, T. Levanen, and M. Valkama, "Fast-convolution filtered OFDM waveforms with adjustable CP length," in *Proc. IEEE Global Conf. Signal Inf. Process. (GlobalSIP*, Greater Washington, DC, USA, Dec. 7–9 2016, pp. 635–639, doi: 10.1109/GLOBALSIP.2016.7905919.

[27] P. M. Djurić and S. M. Kay, "Spectrum estimation and modelling," in *Digital Signal Processing Handbook*, V. K. Madisetti and D. B. W. Boca, Eds. Boca Raton, FL, USA: CRC Press, 1999, ch. 14.

[28] J. S. Bendat and A. G. Piersol, *Random Data: Analysis and Measurement Procedures*. Hoboken, NJ, USA: Wiley, 2010, vol. 4.

Juha Yli-Kaakinen received the Diploma Engineering degree in electrical engineering and the Doctor of Technology degree (Hons.) from the Tampere University of Technology (TUT), Tampere, Finland, in 1998 and 2002, respectively.

From 1995 to 2021, he held various research positions with TUT. He is currently with Nokia Mobile Networks, Finland. His research interests include digital signal processing, especially in digital filter and filter-bank optimization for communication systems and very large scale integration implementations. He has been recognized by the Nokia Mobile Networks Top Inventor Award in 2022.

Toni Levanen received the M.Sc. and D.Sc. degrees from the Tampere University of Technology, Finland, in 2007 and 2014, respectively.

In addition to his contributions in academic research, he has worked in industry on wide variety of development and research projects. He is currently with Nokia Mobile Networks, Finland. His current research interests include physical-layer design for 5G NR, interference modeling in 5G cells, and high-mobility support in millimeter-wave communications.

Arto Palin received the M.Sc. (Tech.) degree from the Tampere University of Technology. He has long industrial experience in wireless technologies, covering cellular networks, broadcast systems, and local area communications. He is currently working as a Principal Silicon Architect.

Markku Renfors (Life Fellow, IEEE) received the D.Tech. degree from the Tampere University of Technology (TUT), Tampere, Finland, in 1982.

Since 1992, he has been a Professor with the Department of Electronics and Communications Engineering, TUT, where he was the Head from 1992 to 2010. He is currently a Professor Emeritus with Tampere University. His research interests include advanced communication waveforms, including filter-bank-based multicarrier systems and signal processing algorithms for flexible communications receivers and transmitters. He was a co-recipient of the Guillemin-Cauer Award (together with T. Saramäki) from the IEEE Circuits and Systems Society in 1987.

Mikko Valkama (Fellow, IEEE) received the D.Sc. (Tech.) degree (Hons.) from the Tampere University of Technology, Finland, in 2001. In 2003, he was with the Communications Systems and Signal Processing Institute, SDSU, San Diego, CA, USA, as a Visiting Research Fellow. He is currently a Full Professor and the Department Head of electrical engineering with the newly formed Tampere University (TAU), Finland. His general research interests include radio communications, radio localization, and radio-based sensing with particular emphasis on 5G and 6G mobile radio networks.